



OPEN ACCESS

EDITED BY

Hua Yang,
Lanzhou University of Technology, China

REVIEWED BY

Fei Wang,
Chongqing University of Technology,
China
Zuming He,
Changzhou University, China
Yuxiang Yan,
Nanjing University, China, in
collaboration with reviewer ZH

*CORRESPONDENCE

Chao Ye,
✉ hi_clover1985@163.com

SPECIALTY SECTION

This article was submitted to
Semiconducting Materials and Devices,
a section of the journal
Frontiers in Materials

RECEIVED 10 March 2023

ACCEPTED 28 March 2023

PUBLISHED 06 April 2023

CITATION

Ye C and Li C (2023), Construction of
BaTiO₃/CeO₂ heterojunction and
comparative study on photocatalytic
activity of degradation of different drugs.
Front. Mater. 10:1183819.
doi: 10.3389/fmats.2023.1183819

COPYRIGHT

© 2023 Ye and Li. This is an open-access
article distributed under the terms of the
[Creative Commons Attribution License
\(CC BY\)](https://creativecommons.org/licenses/by/4.0/). The use, distribution or
reproduction in other forums is
permitted, provided the original author(s)
and the copyright owner(s) are credited
and that the original publication in this
journal is cited, in accordance with
accepted academic practice. No use,
distribution or reproduction is permitted
which does not comply with these terms.

Construction of BaTiO₃/CeO₂ heterojunction and comparative study on photocatalytic activity of degradation of different drugs

Chao Ye^{1*} and Chengui Li²

¹School of Pharmacy, Hebei Medical University, Shijiazhuang, China, ²College of Animal Science and Veterinary Medicine, Shandong Agricultural University, Tai'an, China

A type II band aligned BaTiO₃/CeO₂ photocatalysts was constructed by a simple one-step solution synthesis method. The BaTiO₃/CeO₂ photocatalysts contain only cubic phase BaTiO₃ and CeO₂, and the particles are approximately spherical with a small amount of adhesion and agglomeration, and the average particle size is about 50 nm. Transmission electron microscopy (TEM) observation and element Mapping characterization confirmed the formation of special heterojunction between BaTiO₃ and CeO₂ and the presence of a large number of oxygen vacancies, which resulted in high visible optical absorption coefficient. The BaTiO₃/CeO₂ photocatalysts demonstrated high photocatalytic activity for the degradation of oxytetracycline hydrochloride, and the optimal drug concentration, catalyst content and pH value are 50 mg/L, 1 g/L and 7, respectively. Simultaneously, the BaTiO₃/CeO₂ photocatalysts were selective for degradation of aureomycin hydrochloride, doxycycline hydrochloride and tetracycline hydrochloride. Other photocatalytic experiments show that the BaTiO₃/CeO₂ photocatalysts have high chemical and cyclic stability, and the synergistic effect of holes, hydroxyl radicals and superoxide radicals plays an important role in the whole photocatalytic process. This simple synthesis route provides a technical reference for constructing other wide-band gap semiconductors to respond to simulated sunlight.

KEYWORDS

one-step solution synthesis method, BaTiO₃, CeO₂, oxytetracycline hydrochloride, wide-band gap

1 Introduction

In the process of production and life, human beings depend very much on drugs, especially antibiotics (Verma et al., 2022). When many diseases occur, people use large amounts of antibiotics, but only a small part of these antibiotics are absorbed by the body, most of which will be excreted in the stool (Nazarov, 2022; Li et al., 2023; Wang et al., 2023). If these excluded antibiotics are discharged directly into the environment, it will cause great pollution to the living environment. In the process of aquaculture, in order to make aquaculture products high yield and reduce morbidity, a large number of antibiotics will be used (Okeke et al., 2022; Tong et al., 2022). To reduce the effects of antibiotics on ecological environment and water environment, antibiotics should be degraded from the source.

Photocatalysis is a green technology that can use sunlight to degrade antibiotics, thus reducing environmental pollution (Han et al., 2022; Sahoo et al., 2022; Wang et al., 2022;

Zhang et al., 2022). The key to the photocatalytic degradation of antibiotics is the selection of photocatalyst, and the semiconductor photocatalyst that can respond to visible light should be selected in order to effectively utilize sunlight. Barium titanate (BaTiO_3) and cerium dioxide (CeO_2) are two common photocatalysts, but they can only respond to ultraviolet light because of their large optical band gap (Gu et al., 2022; Xiao et al., 2022; Masekela et al., 2023; Passi and Pal, 2023). Therefore, researchers are focusing on enhancing their light response, especially to simulated sunlight, through ion doping, surface modification, and heterostructural construction (Cheng et al., 2022; Gao et al., 2022; Prajapati et al., 2022). Generally, when heterojunctions are constructed, the coupling of semiconductor materials with a small band gap that can respond to simulated sunlight and semiconductor materials with a wide band gap is selected to enhance the photocatalytic activity of the system (Jing et al., 2022; Masula et al., 2022; Yu et al., 2023). Although BaTiO_3 and CeO_2 have been coupled together, there are no reports of coupling the two to construct special oxygen vacancies to study their photocatalytic activity (Tarasevich and Lebedev, 2010; Khatkhatay et al., 2013; Rehman et al., 2021; Yan et al., 2022a; Yan et al., 2022b).

In this paper, we propose a novel one-step solution synthesis method to construct a type II band aligned $\text{BaTiO}_3/\text{CeO}_2$ photocatalysts and investigate its photocatalytic activity. The phase structure, microstructure, optical properties and photocatalytic activity of $\text{BaTiO}_3/\text{CeO}_2$ photocatalysts were studied by various characterization methods. By studying the effects of different drug concentrations, catalyst contents, pH values and antibiotics on the photocatalytic activity of $\text{BaTiO}_3/\text{CeO}_2$ photocatalyst, the optimal experimental conditions and the mechanism of drug selectivity of $\text{BaTiO}_3/\text{CeO}_2$ photocatalysts were revealed. Based on a series of photocatalytic experiments and band arrangement theory, a reasonable photocatalytic mechanism of $\text{BaTiO}_3/\text{CeO}_2$ photocatalysts for the degradation of drugs has been proposed.

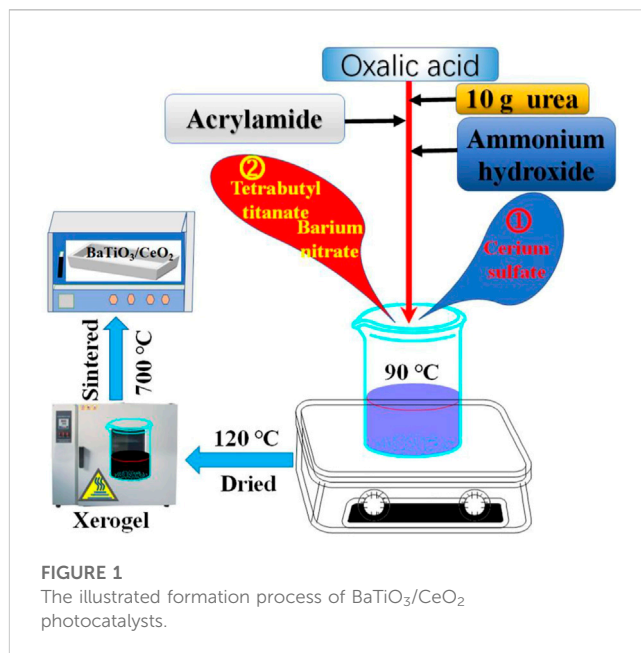
2 Experimental

2.1 Starting materials

Tetrabutyl titanate (CHO_4Ti , 99.5%), barium nitrate ($\text{Ba}(\text{NO}_3)_2$, 99.5%), Cerium sulfate ($\text{Ce}_2(\text{SO}_4)_3 \cdot 8\text{H}_2\text{O}$, 99.5%), oxalic acid ($\text{H}_2\text{C}_2\text{O}_4$, AR), urea ($\text{CO}(\text{NH}_2)_2$, AR), acrylamide ($\text{C}_3\text{H}_5\text{NO}$, AR), and ammonium hydroxide ($\text{NH}_3 \cdot \text{H}_2\text{O}$, AR) were purchased from Aladdin Reagent (Shanghai) Co., Ltd. These reagents are not further purified when used to prepare $\text{BaTiO}_3/\text{CeO}_2$ photocatalysts.

2.2 One step synthesize of $\text{BaTiO}_3/\text{CeO}_2$ photocatalysts

According to the molar ratio of $n_{\text{BaTiO}_3} : n_{\text{CeO}_2} = 1:1$, stoichiometric amounts of CHO_4Ti , $\text{Ba}(\text{NO}_3)_2$ or $\text{Ce}_2(\text{SO}_4)_3 \cdot 8\text{H}_2\text{O}$ were sequential dissolved in a beaker containing 50 mL of deionized water to form a solution of 0.03 mol/L (Relative to metal ions). Subsequently, the dissolution process of the above reagent was observed. After being completely dissolved, 5 g oxalic acid is added to make it fully complex



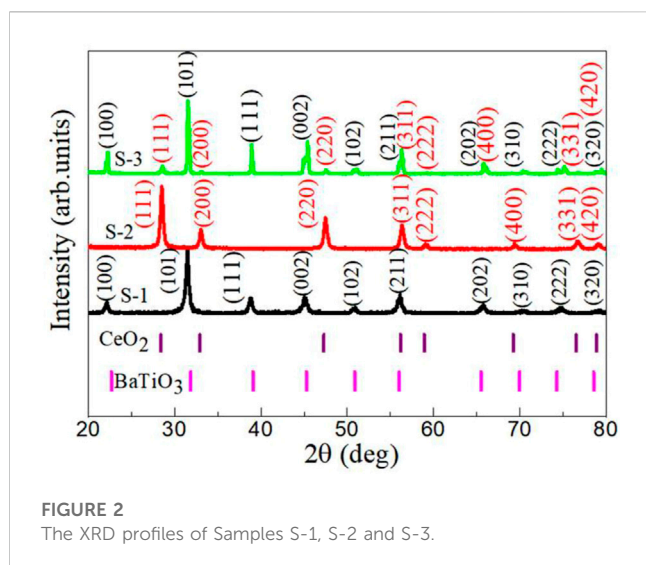
with metal ions to form a complex. After the reagent continued to react uniformly without precipitation, 10 g urea was added as an accelerant. Acrylamide is added within 2 min after the accelerant is added as a network precursor that restricts the free movement of metal ions. After the reagent was completely dissolved, the pH value of the reaction solution was adjusted to 4 with ammonia water, and the deionized water was continuously added to reach 200 mL. After pH is adjusted, heat the oil bath to 90°C until black gel appears. The black gel was then placed in a drying oven to dry at 120°C for 48 h to obtain xerogel. The xerogel was then placed in a tubular sintering furnace at 700°C for 10 h to obtain the final products. Figure 1 shows the illustrated formation process of $\text{BaTiO}_3/\text{CeO}_2$ photocatalysts. For comparison, single-component BaTiO_3 and CeO_2 photocatalysts were synthesized using the same method. The BaTiO_3 , CeO_2 and $\text{BaTiO}_3/\text{CeO}_2$ photocatalysts are marked as Samples S-1, S-2 and S-3, respectively.

2.3 Sample measurement

The BaTiO_3 , CeO_2 and $\text{BaTiO}_3/\text{CeO}_2$ photocatalysts were characterized by X-ray powder diffraction (XRD), performed on a DX-2007BH diffractometer at room temperature to inquire the phase structure and purity. The morphology microstructures of BaTiO_3 , CeO_2 and $\text{BaTiO}_3/\text{CeO}_2$ photocatalysts were recorded by HITACHI S-4800 type field emission scanning electron microscopy (FE-SEM) and JEOL JEM-2100 type high-resolution transmission electron microscopy (TEM). Ultraviolet-visible absorption spectra measurements of BaTiO_3 , CeO_2 and $\text{BaTiO}_3/\text{CeO}_2$ photocatalysts were performed on a UV1901 UV-Visible spectrophotometer.

2.4 Photocatalytic activity measurements

The photocatalytic degradation of oxytetracycline hydrochloride (OH), aureomycin hydrochloride (AH), doxycycline hydrochloride



(DH), or tetracycline hydrochloride (TH) solution by simulated sunlight was studied using BaTiO₃, CeO₂ and BaTiO₃/CeO₂ photocatalysts. The degradation of OH, AH, DH or TH was investigated in a Pyrex beaker under simulated sunlight irradiation by placing the beaker in a Xenon lamp light source. In each experiment, 0.05, 0.10, 0.15 or 0.20 g of BaTiO₃, CeO₂ or BaTiO₃/CeO₂ photocatalysts was added to 100 mL of aqueous solution containing 10, 30, 50, 70 or 90 mg/L drug. Prior to illumination, the above solution was magnetically stirred in the dark for 30 min to disperse the BaTiO₃, CeO₂ or BaTiO₃/CeO₂ photocatalysts and establish an adsorption/desorption equilibrium to exclude the effect of adsorption on photocatalysis. After that, the solution was irradiated with simulated sunlight irradiation. During simulated sunlight irradiation process, magnetically stirring was continuously executed to keep the homogeneous mixture in suspension. Every 30 min, 3 mL of the drug solution was sampled and centrifugated immediately to remove the BaTiO₃, CeO₂ or BaTiO₃/CeO₂ photocatalysts. Then the supernatant solution was analyzed by recording the absorbance curve of the remained drug using a UV-visible spectrophotometer. The degradation percentage of BaTiO₃, CeO₂ or BaTiO₃/CeO₂ photocatalysts is named as $((A_0 - A_t)/A_0) \times 100\%$, where A_0 and A_t are the drug absorbance (OH, AH, DH or TH) before and after simulated sunlight irradiation, respectively. To perform the capture experiment, the ethylenediaminetetraacetic acid disodium salt (EDTA-2Na), isopropyl alcohol (IPA), and p-benzoquinone (BQ) have been used to detect the holes, hydroxyl radicals, and superoxide radicals, respectively. Different from the photocatalytic experiment, the capture experiment requires adding 1 mmol of the trapping agent in the reaction solution.

3 Results and discussions

3.1 Phase structure and purity

The XRD diffraction patterns of BaTiO₃, CeO₂ and BaTiO₃/CeO₂ photocatalysts are displayed in Figure 2. For the Sample S-1,

all peaks indexed as (100), (101), (111), (002), (102), (211), (202), (310), (311), (222), and (320) in XRD patterns are ascribed to cubic BaTiO₃ phase with the space group: Pm-3m (221) according to JCPDS standard card number: 74-1996. The diffraction peaks of Sample S-2 can be indexed as the (111), (200), (220), (311), (222), (400), (331), and (420) planes of CeO₂ with the JCPDS standard card number: 01-071-6329 and the space group: Fm-3m (225), showing their cubic structure. When BaTiO₃/CeO₂ photocatalysts (Sample S-3) are synthesized in one-step synthesis method, the sample contains only the diffraction peaks of BaTiO₃ and CeO₂, but no other impurity peaks. The average crystal size (D) of BaTiO₃, CeO₂ or BaTiO₃/CeO₂ photocatalysts is determined from by broadening the diffraction peaks (111), (101), (211), and (311) plane using Debye-Scherrer's formula (Chavan et al., 2017).

$$D = \frac{k\lambda}{B\cos\theta} \quad (1)$$

Where, k is the constant, $k = 0.9$ is used in the work due to the spherical nanoparticles, λ is the wavelength of the X-ray ($\lambda = 1.5406 \text{ \AA}$), B is the broadening of the diffraction line measured at half maximum intensity, and θ is the diffraction angle. The D values of Samples S-1, S-2 and S-3 were calculated to be 75 nm, 38 nm, and 47 nm, respectively. To further validate the synthesis of nanoscale particles by one-step synthesis method, microstructure characterization is needed.

3.2 Microstructure characterization

Figures 3A–C shows the SEM images of Samples S-1, S-2 and S-3. The BaTiO₃, CeO₂ or BaTiO₃/CeO₂ photocatalysts were nanocrystalline with similar morphology of particles. These particles are approximately spherical, with a few particles showing slight adhesion agglomeration. To calculate the particle size distribution of these nanoparticles, 100 particles from each sample were used for statistics. Figures 3D–F shows the particle size distributions of Samples S-1, S-2 and S-3. The average particle size of Samples S-1, S-2 and S-3 were calculated to be 80 nm, 40 nm, and 50 nm, respectively. The results observed by SEM are similar to those calculated by XRD. Compared with BaTiO₃, the particle size of BaTiO₃/CeO₂ photocatalysts decreased significantly. The main reason for this phenomenon may be that cerium ions affect the coordination environment of barium and titanium ions.

TEM and element Mapping characterization experiments were performed to further confirm the formation of heterojunction between BaTiO₃ and CeO₂. Figure 4A shows the TEM image of Sample S-3. As can be seen from the Figure 4A, the outlines of large particles and fine particles are very clear, consistent with SEM observation results. Figure 4B shows the high-resolution TEM (HRTEM) image of Sample S-3. The interplanar spacing of large and fine particles is 0.28 nm and 0.31 nm, respectively, corresponding to the (101) crystal plane of BaTiO₃ and the (111) crystal plane of CeO₂. The BaTiO₃ particles and CeO₂ particles are closely connected, forming a special heterojunction structure. To further explore the heterojunction formed between BaTiO₃ and CeO₂, the relevant BF-TEM, EDS layered images and element Mapping images are given in Figures 4C–H. It can be seen from the figure that CeO₂ is evenly dispersed on the BaTiO₃ parent,

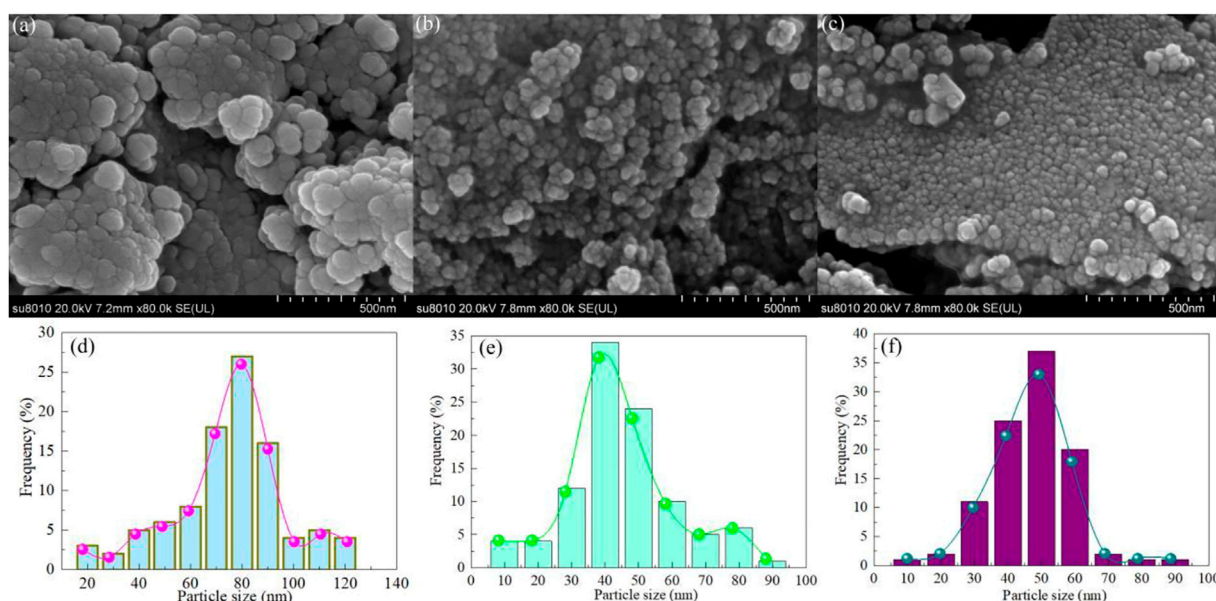


FIGURE 3
The SEM images of Samples (A) S-1, (B) S-2 and (C) S-3. Particle size distributions of Samples (D) S-1, (E) S-2 and (F) S-3.

indicating that a heterojunction is formed between BaTiO_3 and CeO_2 .

3.3 Optical properties and E_g values

Figure 5A shows the UV-vis absorption spectra of Samples S-1, S-2 and S-3. In the range of 230 nm–800 nm, the optical absorption coefficients of the three samples decreased with the increase of wavelength. In the UV range, Sample S-2 has the highest optical absorption coefficient, Sample S-1 has the lowest optical absorption coefficient. In the visible range, Sample S-3 has a high optical absorption coefficient, which may be caused by the appearance of a large amount of surface defect oxygen at the interface of BaTiO_3 and CeO_2 after the formation of heterojunction (Yu et al., 2023). This phenomenon will be conducive to $\text{BaTiO}_3/\text{CeO}_2$ photocatalyst producing visible light photocatalytic activity for degradation of drugs. Figures 5B–D shows the estimated band gap (E_g) of Samples S-1, S-2 and S-3. The E_g values of Samples S-1, S-2 and S-3 were calculated to be 3.06, 3.15, and 2.92 eV, respectively. In general, two semiconductors coupled together do not change the E_g value of the main lattice. However, when BaTiO_3 and CeO_2 are coupled, the obvious decrease of E_g value may be due to the presence of a large amount of surface defect oxygen at the interface of the two.

3.4 Photocatalytic activity

Figure 6A shows the photocatalytic oxytetracycline hydrochloride (OH) degradation over BaTiO_3 , CeO_2 and $\text{BaTiO}_3/\text{CeO}_2$ photocatalysts under visible light irradiation. In order to verify whether OH can be degraded without photocatalyst under visible light irradiation conditions, blank experiments were performed.

After 3 h of light exposure, OH without catalyst is difficult to be degraded by visible light, indicating that OH is difficult to be degraded naturally under visible light conditions. With the increase of the time of visible light, the degradation rate of OH in all samples increased continuously. The photocatalytic degradation rate of BaTiO_3 and CeO_2 with single component is very low, while the photocatalytic degradation rate of $\text{BaTiO}_3/\text{CeO}_2$ composite photocatalyst is the highest. Figure 6B shows the $-\ln(A_t/A_0) \sim$ time curve for the photodegradation of OH over BaTiO_3 , CeO_2 and $\text{BaTiO}_3/\text{CeO}_2$ photocatalysts. It shows a good linear relationship between $-\ln(A_t/A_0)$ and time. First-order rate constant (k) for the photodegradation of OH over BaTiO_3 , CeO_2 and $\text{BaTiO}_3/\text{CeO}_2$ photocatalysts as displayed in Figure 6C. The k values of BaTiO_3 , CeO_2 and $\text{BaTiO}_3/\text{CeO}_2$ photocatalysts are 0.00379, 0.00486 and 0.01248 min^{-1} , respectively. The degradation rate of $\text{BaTiO}_3/\text{CeO}_2$ photocatalysts is 15.80 times that of the blank experiment, and 3.29 times that of BaTiO_3 . Figure 6D shows the degradation percentage for the photodegradation of OH over BaTiO_3 , CeO_2 and $\text{BaTiO}_3/\text{CeO}_2$ photocatalysts. The degradation percentage of BaTiO_3 , CeO_2 and $\text{BaTiO}_3/\text{CeO}_2$ photocatalysts are 51%, 61%, and 91%, respectively. The results showed that the $\text{BaTiO}_3/\text{CeO}_2$ photocatalysts showed high photocatalytic activity for the degradation of OH.

The photocatalytic activity of photocatalyst is affected by drug concentration, catalyst content and pH value. Figure 7A shows the OH degradation yields at different drug concentrations. With the increase of drug yields at different drug concentrations, the degradation percentage of $\text{BaTiO}_3/\text{CeO}_2$ photocatalysts initially increased with the increase of drug concentration, but decreased with the increase of drug concentration when the drug concentration reached 50 mg/L. The reason why the photocatalytic activity decreases under high drug concentration is mainly due to the shielding effect of light, which reduces the chance of photogenerated carrier generation

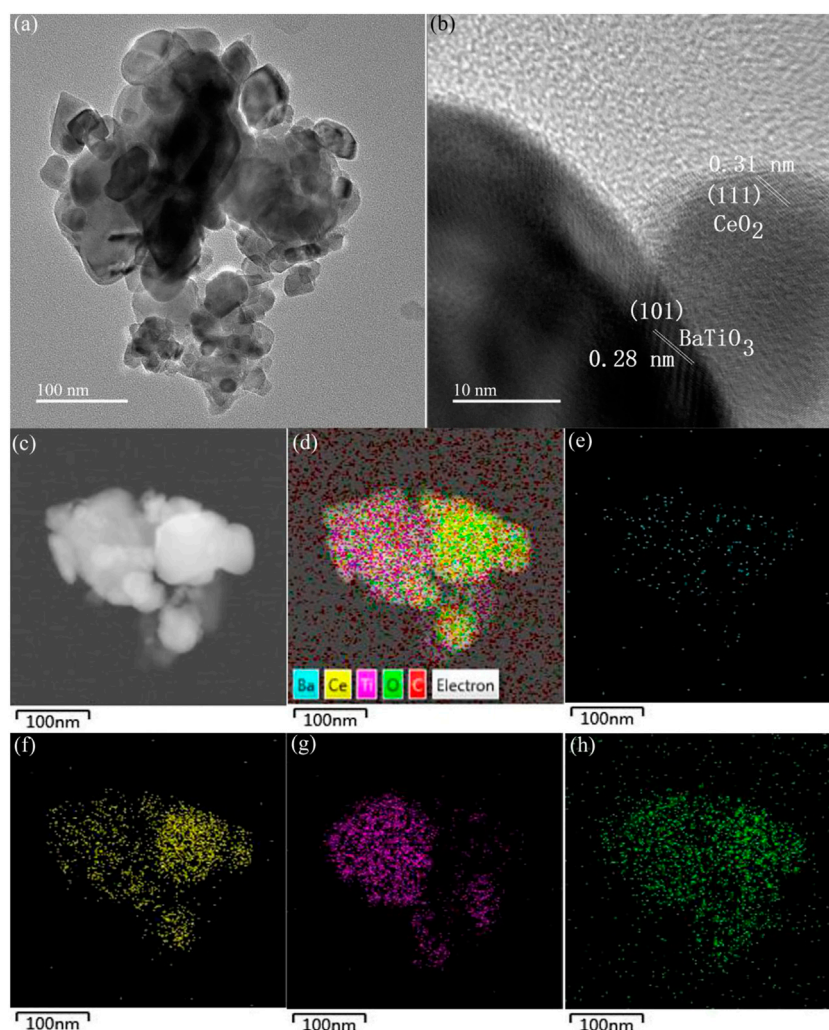
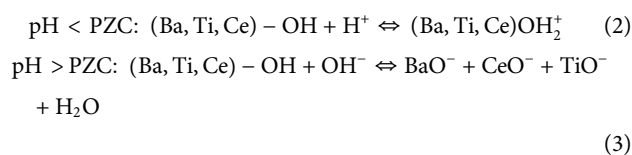


FIGURE 4

(A) TEM, (B) HRTEM, (C) BF-TEM, (D) EDS layered images of Sample S-3. The elemental maps of the region shown in panel (C). (E) Ba, (F) Ti, (G) Ce and (H) O.

(Kaur et al., 2016). As can be seen from Figure 7A, the optimal drug concentration is 50 mg/L. Figure 7B shows the OH degradation yields at different catalyst contents. Similar to the concentration of different drugs, the photocatalytic activity of BaTiO₃/CeO₂ photocatalysts firstly increased and then decreased with the increase of catalyst content. When the concentration of photocatalyst is too high, the path length of photon entering the reaction solution becomes longer due to the light scattering effect, and the separation and transfer rate of photogenerated carrier decreases, which leads to the decrease of photocatalytic activity (Hiragond et al., 2022). The optimal catalyst content was 1 g/L of BaTiO₃/CeO₂ photocatalysts for the degradation of OH. Figure 7C shows the OH degradation yields at different pH values. It can be seen from the figure that the BaTiO₃/CeO₂ photocatalysts showed the highest photocatalytic activity in the degradation of OH under neutral and alkaline conditions. The main reason for this phenomenon is that the charge states on the surface of BaTiO₃/CeO₂ photocatalysts and drug molecules show different electrical properties under different acid-base conditions. To verify this

hypothesis, Figure 7D shows the pH value of the reaction solution before and after photocatalysis. The PZC value of BaTiO₃/CeO₂ photocatalysts is 6.18. Under acidic conditions, the degradation rate of BaTiO₃/CeO₂ photocatalysts is significantly lower than that of basic conditions. In the neutral and basic condition, the degradation rate of BaTiO₃/CeO₂ photocatalysts reached the maximum, which was basically consistent with the value of PZC. When pH < PZC, the surface of BaTiO₃/CeO₂ photocatalysts presents positive charge, while when pH > PZC presents negative charge (Zeng, 2011; Mahamud et al., 2023). The BaTiO₃/CeO₂ photocatalysts can degrade OH in a neutral and basic environment. The relevant chemical expression can be described as follows:



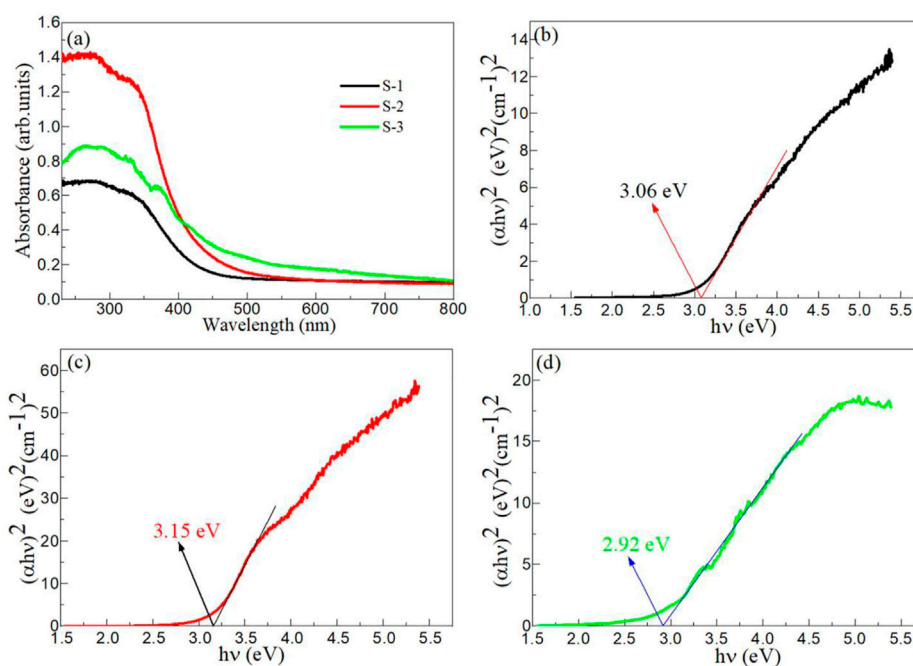


FIGURE 5

(A) UV-vis absorption spectra of Samples S-1, S-2 and S-3. The estimated band gap of Samples (B) S-1, (C) S-2 and (D) S-3.

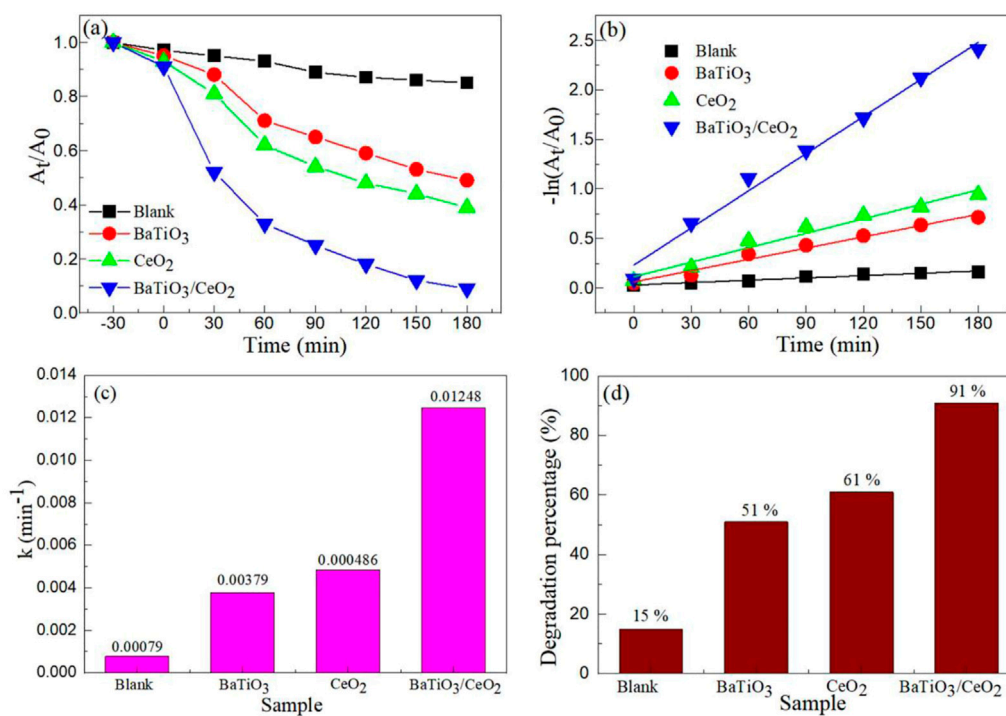


FIGURE 6

(A) Photocatalytic oxytetracycline hydrochloride (OH) degradation over BaTiO₃, CeO₂ and BaTiO₃/CeO₂ photocatalysts under visible light irradiation. (B) $-\ln(A_t/A_0) \sim$ time curve, (C) First-order rate constants and (D) Degradation percentage for the photodegradation of OH over BaTiO₃, CeO₂ and BaTiO₃/CeO₂ photocatalysts.

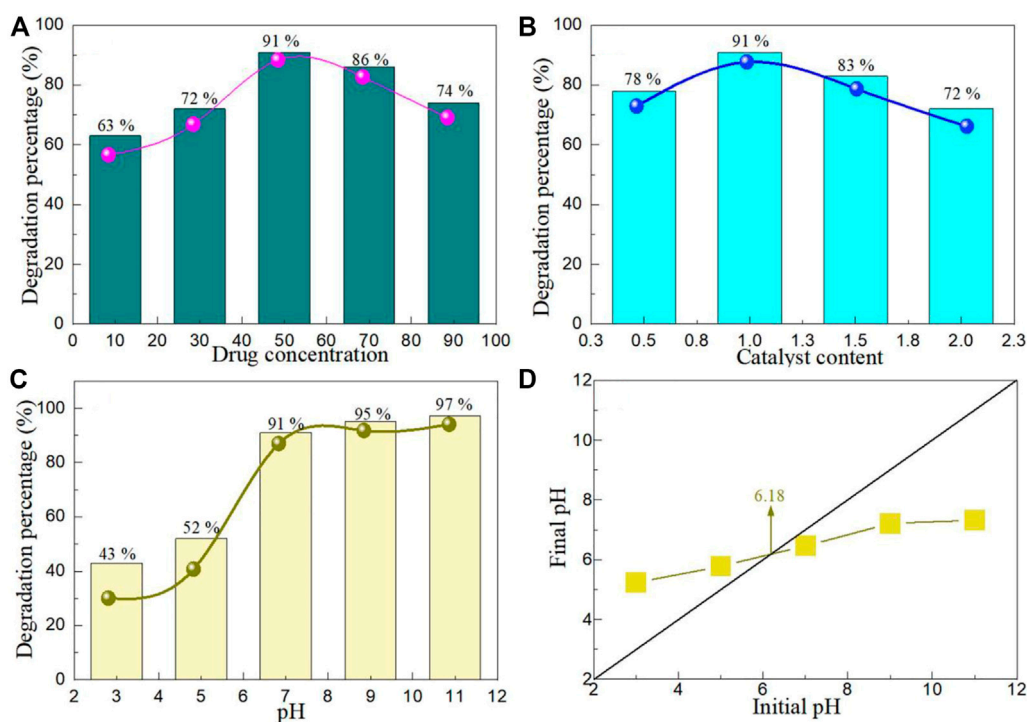


FIGURE 7

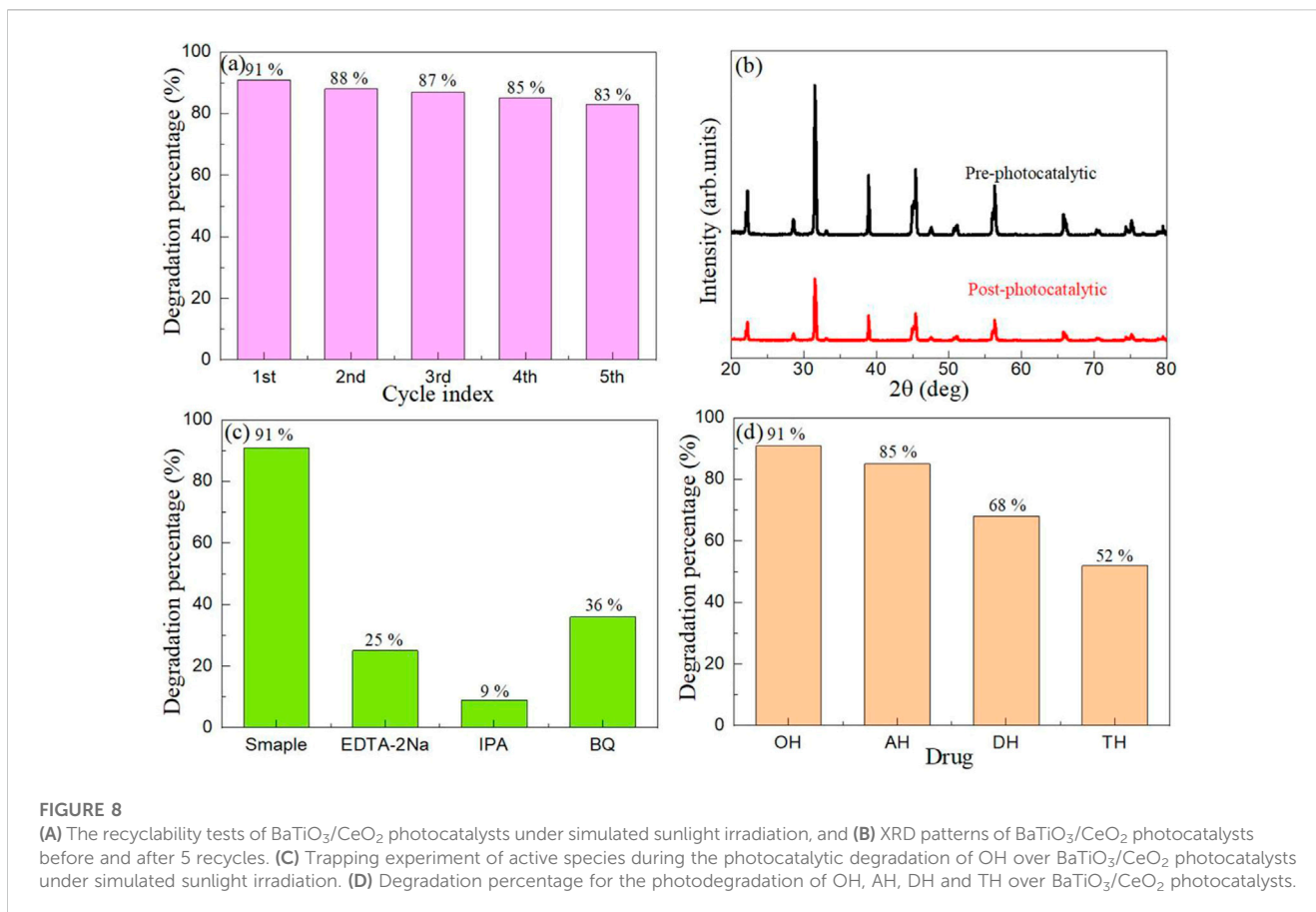
OH degradation yields at (A) different drug concentrations, (B) different catalyst contents, (C) different pH values. (D) The pH value of the reaction solution before and after photocatalysis.

The photocatalyst needs high stability and reuse to be used in industrial applications. In order to prove that the BaTiO₃/CeO₂ photocatalysts can be applied commercially, Figure 8A shows the recyclability tests of BaTiO₃/CeO₂ photocatalysts under simulated sunlight irradiation. Before each reuse experiment, the catalyst used last time will be centrifuged, separated, filtered, dried and sintered at low temperature before the next photocatalytic experiment is performed. After five cycles, the degradation percentage of BaTiO₃/CeO₂ photocatalyst decreased by only 8%, indicating that the catalyst could be recycled. The slight decrease in degradation percentage can be attributed to the loss of photocatalyst during use. Figure 8B shows the XRD patterns of BaTiO₃/CeO₂ photocatalysts before and after 5 recycles. Except for the change in the intensity of the diffraction peak, the position of the diffraction peak of BaTiO₃/CeO₂ photocatalysts did not change, which confirmed that the catalyst was stable and would not decompose into other oxides after repeated use.

The high photocatalytic activity of BaTiO₃/CeO₂ photocatalysts may be due to the synergistic action of various free radicals, which makes its photocatalytic activity higher than that of single component BaTiO₃ and CeO₂. To confirm this conjecture, Figure 8C shows the trapping experiment of active species during the photocatalytic degradation of OH over BaTiO₃/CeO₂ photocatalysts under simulated sunlight irradiation. The ethylenediaminetetraacetic acid disodium salt (EDTA-2Na), isopropyl alcohol (IPA), and p-benzoquinone (BQ) have been used to detect the holes, hydroxyl radicals, and superoxide radicals, respectively. The only difference between the free radical

capture experiment and the photocatalysis experiment is that 1 mmol of the trapping agent needs to be added to the reaction solution before the photocatalysis. As can be seen from the Figure 8C, after the addition of EDTA-2Na, IPA and BQ to the BaTiO₃/CeO₂ photocatalysts, the photocatalytic activity decreased significantly, indicating that holes, hydroxyl radicals and superoxide radicals all played an important role in the whole photocatalytic process.

In order to explore that the BaTiO₃/CeO₂ photocatalysts can degrade other drugs of the same type as OH, the drugs including AH, DH and TH were also selected to perform photocatalytic experiments. Figure 8D shows the degradation percentage for the photodegradation of OH, AH, DH and TH over BaTiO₃/CeO₂ photocatalysts. It can be seen from the figure that all BaTiO₃/CeO₂ photocatalysts can degrade OH, AH, DH and TH drugs, but the degradation percentage decreases successively. This may be related to the number of -OH groups contained in these drugs, the number of Cl ions, and the location of N-H functional groups at different locations in the carbon ring. From the perspective of molecular structure of different drugs, the preference of BaTiO₃/CeO₂ photocatalysts for different functional groups led to the obvious difference in the percentage of photocatalytic degradation. On the other hand, the pH of different drug molecules is different. When reacting with photocatalyst, the electrical properties of the surface molecular charge are obviously different, resulting in different percentage of photocatalytic degradation. The results showed that the BaTiO₃/CeO₂ photocatalysts was selective to the degradation of drugs.



3.5 Photocatalytic mechanism

It can be seen from the photocatalytic experiments, cyclic stability experiments and capture experiments that the BaTiO₃/CeO₂ photocatalysts has high photocatalytic degradation activity for the degradation of OH under the simulated sunlight irradiation. Based on the capture experiment, it can be seen that hole, hydroxyl radical and superoxide radical play an important role. These important roles need to be further confirmed by theoretical research. The BaTiO₃/CeO₂ photocatalysts showed high photocatalytic activity in the degradation of OH, and its mechanism could be analyzed in combination with the energy band theory. Based on formulas 4, 5 (He et al., 2021; He et al., 2023a), conduction band potential (E_{CB}) and valence band potential (E_{VB}) of BaTiO₃ and CeO₂ can be obtained.

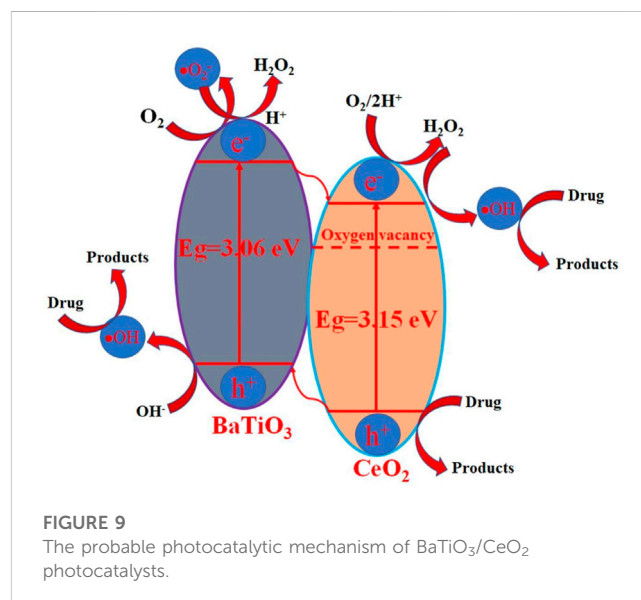
$$E_{CB} = X - E^{\circ} - 0.5E_g \quad (4)$$

$$E_{VB} = E_{CB} + E_g \quad (5)$$

Where, the E_g values for the BaTiO₃ and CeO₂ is 3.06 eV and 3.15 eV, respectively. E° is 4.5 eV. According to the formulas 6, 7, the X values for the BaTiO₃ and CeO₂ are 5.13 eV and 5.55 eV, respectively.

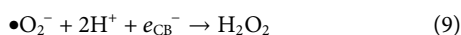
$$X(\text{BaTiO}_3) = \sqrt[3]{X(\text{Ba}) \cdot X(\text{Ti}) \cdot X(\text{O})^3} \quad (6)$$

$$X(\text{CeO}_2) = \sqrt[3]{X(\text{Ce}) \cdot X(\text{O})^2} \quad (7)$$

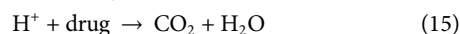
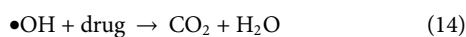
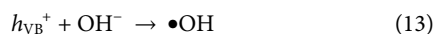


Based on this calculation, the E_{CB} values of BaTiO₃ and CeO₂ are -0.90 eV and -0.53 eV, respectively, while the E_{VB} values of BaTiO₃ and CeO₂ are 2.16 eV and 2.62 eV, respectively. According to the results of the above calculation, an energy level diagram can be proposed as shown in Figure 9. It can be seen from the figure that the

combination of BaTiO₃ and CeO₂ forms a type II band arrangement, which is conducive to the transfer and separation of photogenic carriers. However, the band gap values of BaTiO₃ and CeO₂ of a single component are large, which is difficult to respond to visible light. When the two are combined together, they form defect structures such as vacancies, which make it possible to respond to simulated sunlight and promote the transfer and separation of electron and hole pairs. In the conduction band, since the redox potential of O₂/•O₂⁻ is -0.13 V, (Arai et al., 2007), the following reactions can occur:



In the valence band, the following chemical reactions can occur due to the redox potentials of H₂O/•OH and OH⁻/•OH are +2.72 V and +1.89 V versus NHE: (Tachikawa et al., 2007; He et al., 2022; He et al., 2023b):



According to the above analysis, the hole, hydroxyl and superoxide radicals promote the degradation of drug over BaTiO₃/CeO₂ photocatalysts. This way of vacancy construction can promote the application of semiconductor materials with large band gap values in the field of visible light photocatalysis.

4 Conclusion

A simple one-step solution synthesis method was used to construct a type II band aligned BaTiO₃/CeO₂ photocatalysts. XRD characterization confirms that the obtained BaTiO₃/CeO₂ photocatalysts contains only cubic phase BaTiO₃ and CeO₂ diffraction peaks. SEM observation showed that the BaTiO₃/CeO₂ photocatalysts were spherical particles with an average particle size of about 50 nm. TEM measurements confirmed the formation of special heterojunction between BaTiO₃ and CeO₂. The optical absorption coefficient of BaTiO₃/CeO₂ photocatalysts

in the visible range is greatly improved due to the presence of oxygen vacancy compared with that of single component BaTiO₃ and CeO₂. The BaTiO₃/CeO₂ photocatalysts demonstrated high photocatalytic activity for the degradation of OH drugs due to the synergistic effect of holes, hydroxyl radicals and superoxide radicals.

Data availability statement

The raw data supporting the conclusion of this article will be made available by the authors, without undue reservation.

Author contributions

All authors listed have made a substantial, direct, and intellectual contribution to the work and approved it for publication.

Funding

This work was supported by the Science and Technology Research Project of Hebei Higher Education Institutions (No. QN2020200) and the Hebei Province Natural Science Fund (No. H2022206517).

Conflict of interest

The authors declare that the research was conducted in the absence of any commercial or financial relationships that could be construed as a potential conflict of interest.

Publisher's note

All claims expressed in this article are solely those of the authors and do not necessarily represent those of their affiliated organizations, or those of the publisher, the editors and the reviewers. Any product that may be evaluated in this article, or claim that may be made by its manufacturer, is not guaranteed or endorsed by the publisher.

References

- Arai, T., Yanagida, M., Konishi, Y., Iwasaki, Y., Sugihara, H., and Sayama, K. (2007). Efficient complete oxidation of acetaldehyde into CO₂ over CuBi₂O₄/WO₃ composite photocatalyst under visible and UV light irradiation. *J. Phys. Chem. C* 111 (21), 7574–7577. doi:10.1021/jp0725533
- Chavan, P., Naik, L. R., Belavi, P. B., Chavan, G., Ramesha, C. K., and Kotnala, R. K. (2017). Studies on electrical and magnetic properties of Mg-substituted nickel ferrites. *J. Electron. Mater.* 46, 188–198. doi:10.1007/s11664-016-4886-6
- Cheng, Z., Luo, S., Liu, Z., Zhang, Y., Liao, Y., Guo, M., et al. (2022). Visible-light-driven hierarchical porous CeO₂ derived from wood for effective photocatalytic degradation of methylene blue. *Opt. Mater.* 129, 112429. doi:10.1016/j.optmat.2022.112429
- Gao, X., Li, B., and Jian, S. (2022). Step-scheme CeO₂/CaIn₂S₄ heterostructured photocatalysts for efficient reduction of Cr(VI) under visible light. *Colloids Surfaces A Physicochem. Eng. Aspects* 648, 129168. doi:10.1016/j.colsurfa.2022.129168
- Gu, J., Liu, H., Peng, T., Li, S., Xu, L., Zhang, J., et al. (2022). Ag@ CeO₂-Au nanorod plasmonic nanohybrids for enhanced photocatalytic conversion of benzyl alcohol to benzaldehyde. *ACS Appl. Nano Mater.* 5 (4), 4972–4982. doi:10.1021/acsnm.1c04563
- Han, M., Wang, S., Chen, X., Liu, H., Gao, H., Zhao, X., et al. (2022). Spinel CuB₂O₄ (B= Fe, Cr, and Al) oxides for selective adsorption of Congo red and photocatalytic removal of antibiotics. *ACS Appl. Nano Mater.* 5 (8), 11194–11207. doi:10.1021/acsnm.2c02349
- He, Z., Fareed, H., Yang, H., Xia, Y., Su, J., Wang, L., et al. (2023). Mechanistic insight into the charge carrier separation and molecular oxygen activation of manganese doping BiOBr hollow microspheres. *J. Colloid Interface Sci.* 629, 355–367. doi:10.1016/j.jcis.2022.08.164
- He, Z., Siddique, M. S., Yang, H., Xia, Y., Su, J., Tang, B., et al. (2022). Novel Z-scheme In₂S₃/Bi₂WO₆ core-shell heterojunctions with synergistic enhanced photocatalytic

- degradation of tetracycline hydrochloride. *J. Clean. Prod.* 339, 130634. doi:10.1016/j.jclepro.2022.130634
- He, Z., Yang, H., Su, J., Xia, Y., Fu, X., Wang, L., et al. (2021). Construction of multifunctional dual Z-scheme composites with enhanced photocatalytic activities for degradation of ciprofloxacin. *Fuel* 294, 120399. doi:10.1016/j.fuel.2021.120399
- He, Z., Yang, H., Wong, N. H., Sunarso, J., Huang, Z., Xia, Y., et al. (2023). Construction of $\text{Cu}_7\text{S}_4@ \text{CuCo}_2\text{O}_4$ yolk-shell microspheres composite and elucidation of its enhanced photocatalytic activity, mechanism, and pathway for carbamazepine degradation. *Small* 49, 2207370. doi:10.1002/smll.202207370
- Hiragond, C. B., Powar, N. S., and Lee, J. S. I. (2022). Single-atom catalysts (SACs) for photocatalytic CO_2 reduction with H_2O : Activity, product selectivity, stability, and surface chemistry. *Small* 18 (29), 2201428. doi:10.1002/smll.202201428
- Jing, P., He, C., Huang, S., Li, H., Liu, J., Cui, Y., et al. (2022). 2D Z-scheme heterojunction and oxygen deficiency synergistically boosting the photocatalytic activity of a layered $\text{BaTiO}_3/\text{BiOIO}_3$ composite. *Appl. Mater. Today* 29, 101574. doi:10.1016/j.apmt.2022.101574
- Kaur, A., Umar, A., and Kansal, S. K. (2016). Heterogeneous photocatalytic studies of analgesic and non-steroidal anti-inflammatory drugs. *Appl. Catal. A General* 510, 134–155. doi:10.1016/j.apcata.2015.11.008
- Khatkhatay, F., Chen, A., Lee, J. H., Zhang, W., Abdel-Raziq, H., and Wang, H. (2013). Ferroelectric properties of vertically aligned nanostructured $\text{BaTiO}_3\text{-CeO}_2$ thin films and their integration on silicon. *ACS Appl. Mater. Interfaces* 5 (23), 12541–12547. doi:10.1021/am403834k
- Li, M., Wang, S., Gao, H., Yin, Z., Chen, C., Yang, H., et al. (2023). Selective removal of antibiotics over $\text{MgAl}_2\text{O}_4/\text{C}_3\text{N}_4/\text{YMnO}_3$ photocatalysts: Performance prediction and mechanism insight. *J. Am. Ceram. Soc.* 106 (4), 2420–2442. doi:10.1111/jace.18946
- Mahamud, M., Tadesse, A. M., Bogale, Y., and Bezu, Z. (2023). Zeolite supported $\text{CdS}/\text{TiO}_2/\text{CeO}_2$ composite: Synthesis, characterization and photocatalytic activity for methylene blue dye degradation. *Mater. Res. Bull.* 161, 112176. doi:10.1016/j.materresbull.2023.112176
- Masekela, D., Hintsho-Mbita, N. C., and Mabuba, N. (2023). Application of a piezocatalytic thin film ($\text{FTO}/\text{BaTiO}_3/\text{SnO}_2$) for enhanced degradation of organic pollutants and disinfection of wastewater. *Ceram. Int.* 49 (5), 7566–7579. doi:10.1016/j.ceramint.2022.10.251
- Masula, K., Bhongiri, Y., Rao, G. R., Kumar, P. V., Pola, S., and Basude, M. (2022). Evolution of photocatalytic activity of $\text{CeO}_2\text{-Bi}_2\text{O}_3$ composite material for wastewater degradation under visible-light irradiation. *Opt. Mater.* 126, 112201. doi:10.1016/j.optmat.2022.112201
- Nazarov, P. A. (2022). MDR pumps as crossroads of resistance: Antibiotics and bacteriophages. *Antibiotics* 11 (6), 734. doi:10.3390/antibiotics11060734
- Okeke, E. S., Chukwudozie, K. I., Nyaruaba, R., Ita, R. E., Oladipo, A., Ejeromedoghene, O., et al. (2022). Antibiotic resistance in aquaculture and aquatic organisms: A review of current nanotechnology applications for sustainable management. *Environ. Sci. Pollut. Res.* 29 (46), 69241–69274. doi:10.1007/s11356-022-22319-y
- Passi, M., and Pal, B. (2023). Design of a novel $\text{Ag-BaTiO}_3/\text{GO}$ ternary nanocomposite with enhanced visible-light driven photocatalytic performance towards mitigation of carcinogenic organic pollutants. *Sep. Purif. Technol.* 308, 122839. doi:10.1016/j.seppur.2022.122839
- Prajapati, P. K., Malik, A., Nandal, N., Pandita, S., Singh, R., Bhandari, S., et al. (2022). Morphology controlled Fe and Ni-doped CeO_2 nanorods as an excellent heterojunction photocatalyst for CO_2 reduction. *Appl. Surf. Sci.* 588, 152912. doi:10.1016/j.apsusc.2022.152912
- Rehman, S., Kim, H., Patil, H., Kadam, K. D., Sagar, R. U. R., Aziz, J., et al. (2021). Current rectification, resistive switching, and stable NDR effect in $\text{BaTiO}_3/\text{CeO}_2$ heterostructure devices. *Adv. Electron. Mater.* 7 (6), 2001237. doi:10.1002/aelm.202001237
- Sahoo, R. K., Manna, A. K., Das, A., Mitra, A., Mohapatra, M., Sarangi, S. N., et al. (2022). Facile synthesis of Super-paramagnetic $\text{Au}@ \alpha\text{-Fe}_2\text{O}_3$ hybrid nanoparticle and its assembly on graphene substrate for visible light photo-catalysis. *Appl. Surf. Sci.* 577, 151954. doi:10.1016/j.apsusc.2021.151954
- Tachikawa, T., Fujitsuka, M., and Majima, T. (2007). Mechanistic insight into the TiO_2 photocatalytic reactions: Design of new photocatalysts. *J. Phys. Chem. C* 111 (14), 5259–5275. doi:10.1021/jp069005u
- Tarasevich, T. V., and Lebedev, S. A. (2010). Microstructure and dielectric properties of $\text{BaTiO}_3\text{-CeO}_2\text{-SnO}_2$ ceramics. *Inorg. Mater.* 46, 79–84. doi:10.1134/s0020168510010188
- Tong, B., Shi, L., and Liu, X. (2022). Sol–gel synthesis and photocatalytic activity of graphene oxide/ ZnFe_2O_4 -based composite photocatalysts. *Front. Mater.* 9, 934759. doi:10.3389/fmats.2022.934759
- Verma, T., Aggarwal, A., Singh, S., Sharma, S., and Sarma, S. J. (2022). Current challenges and advancements towards discovery and resistance of antibiotics. *J. Mol. Struct.* 1248, 131380. doi:10.1016/j.molstruc.2021.131380
- Wang, S., Chen, X., Fang, L., Gao, H., Han, M., Chen, X., et al. (2022). Double heterojunction $\text{CQDs}/\text{CeO}_2/\text{BaFe}_{12}\text{O}_{19}$ magnetic separation photocatalysts: Construction, structural characterization, dye and POPs removal, and the interrelationships between magnetism and photocatalysis. *Nucl. Anal.* 1 (3), 100026. doi:10.1016/j.nucana.2022.100026
- Wang, S., Li, M., Gao, H., Yin, Z., Chen, C., Yang, H., et al. (2023). Construction of $\text{CeO}_2/\text{YMnO}_3$ and $\text{CeO}_2/\text{MgAl}_2\text{O}_4/\text{YMnO}_3$ photocatalysts and adsorption of dyes and photocatalytic oxidation of antibiotics: Performance prediction, degradation pathway and mechanism insight. *Appl. Surf. Sci.* 608, 154977. doi:10.1016/j.apsusc.2022.154977
- Xiao, S., Zhang, N., Tao, Y., Song, X., Li, G., Li, H., et al. (2022). Carbon nanotube-threaded mesocrystalline CeO_2 for enhanced photocatalytic NO removal. *ACS Appl. Nano Mater.* 5 (3), 3581–3590. doi:10.1021/acsnm.1c04210
- Yan, X., He, H., Liu, G., Zhao, Z., Pei, Y., Liu, P., et al. (2022). A robust memristor based on epitaxial vertically aligned nanostructured $\text{BaTiO}_3\text{-CeO}_2$ films on silicon. *Adv. Mater.* 34 (23), 2110343. doi:10.1002/adma.202110343
- Yan, X., Yan, H., Liu, G., Zhao, J., Zhao, Z., Wang, H., et al. (2022). Silicon-based epitaxial ferroelectric memristor for high temperature operation in self-assembled vertically aligned $\text{BaTiO}_3\text{-CeO}_2$ films. *Nano Res.* 15 (10), 9654–9662. doi:10.1007/s12274-022-4604-z
- Yu, C., Wang, S., Zhang, K., Li, M., Gao, H., Zhang, J., et al. (2023). Visible-light-enhanced photocatalytic activity of $\text{BaTiO}_3/\gamma\text{-Al}_2\text{O}_3$ composite photocatalysts for photodegradation of tetracycline hydrochloride. *Opt. Mater.* 135, 113364. doi:10.1016/j.optmat.2022.113364
- Zeng, M. (2011). Surface reaction characteristics at low temperature synthesis BaTiO_3 particles by barium hydroxide aqueous solution and titanium tetraisopropoxide. *Appl. Surf. Sci.* 257 (15), 6636–6643. doi:10.1016/j.apsusc.2011.02.090
- Zhang, M., Chen, X., Zu, M., Tang, Y., Liu, C., Li, W., et al. (2022). Synthesis of fibrous micro-nano hierarchical porous cerium dioxide materials by the impregnation and thermal decomposition method and its enhanced photocatalytic activity. *Front. Mater.* 8, 775027.